

7-1-2023

Modulation recognition of low-SNR UAV radar signals based on bispectral slices and GA-BP neural network

Xuemin Liu

Yaoliang Song

Kuiyu Chen

Shihao Yan

Edith Cowan University

Si Chen

See next page for additional authors

Follow this and additional works at: <https://ro.ecu.edu.au/ecuworks2022-2026>



Part of the [Information Security Commons](#)

[10.3390/drones7070472](https://doi.org/10.3390/drones7070472)

Liu, X., Song, Y., Chen, K., Yan, S., Chen, S., & Shi, B. (2023). Modulation recognition of low-SNR UAV radar signals based on bispectral slices and GA-BP neural network. *Drones*, 7(7), article 472. <https://doi.org/10.3390/drones7070472>


This Journal Article is posted at Research Online.
<https://ro.ecu.edu.au/ecuworks2022-2026/2963>

Authors

Xuemin Liu, Yaoliang Song, Kuiyu Chen, Shihao Yan, Si Chen, and Baihua Shi

Article

Modulation Recognition of Low-SNR UAV Radar Signals Based on Bispectral Slices and GA-BP Neural Network

Xuemin Liu ^{1,*}, Yaoliang Song ¹, Kuiyu Chen ¹, Shihao Yan ², Si Chen ¹ and Baihua Shi ¹ 

¹ School of Electronic Engineering and Optoelectronic Technology, Nanjing University of Science and Technology, No. 200 Xiaolingwei Street, Xuanwu District, Nanjing 210000, China; ylsong@njust.edu.cn (Y.S.); cky@njust.cn (K.C.); chensi354@njust.edu.cn (S.C.); shih56h@foxmail.com (B.S.)

² School of Science (Cyber Security), Edith Cowan University, Joondalup 6027, Australia; s.yan@ecu.edu.au

* Correspondence: liuxm@njust.edu.cn; Tel.: +86-189-5168-2415

Abstract: In this paper, we address the challenge of low recognition rates in existing methods for radar signals from unmanned aerial vehicles (UAV) with low signal-to-noise ratios (SNRs). To overcome this challenge, we propose the utilization of the bispectral slice approach for accurate recognition of complex UAV radar signals. Our approach involves extracting the bispectral diagonal slice and the maximum bispectral amplitude horizontal slice from the bispectrum amplitude spectrum of the received UAV radar signal. These slices serve as the basis for subsequent identification by calculating characteristic parameters such as convexity, box dimension, and sparseness. To accomplish the recognition task, we employ a GA-BP neural network. The significant variations observed in the bispectral slices of different signals, along with their robustness against Gaussian noise, contribute to the high separability and stability of the extracted bispectral convexity, bispectral box dimension, and bispectral sparseness. Through simulations involving five radar signals, our proposed method demonstrates superior performance. Remarkably, even under challenging conditions with an SNR as low as -3 dB, the recognition accuracy for the five different radar signals exceeds 90%. Our research aims to enhance the understanding and application of modulation recognition techniques for UAV radar signals, particularly in scenarios with low SNRs.

Keywords: UAV radar signals; low signal-to-noise ratios; bispectral slice; convexity; box dimension; sparseness; neural network



Citation: Liu, X.; Song, Y.; Chen, K.; Yan, S.; Chen, S.; Shi, B. Modulation Recognition of Low-SNR UAV Radar Signals Based on Bispectral Slices and GA-BP Neural Network. *Drones* **2023**, *7*, 472. <https://doi.org/10.3390/drones7070472>

Academic Editor: Emmanouel T. Michailidis

Received: 30 May 2023

Revised: 5 July 2023

Accepted: 14 July 2023

Published: 18 July 2023



Copyright: © 2023 by the authors. Licensee MDPI, Basel, Switzerland. This article is an open access article distributed under the terms and conditions of the Creative Commons Attribution (CC BY) license (<https://creativecommons.org/licenses/by/4.0/>).

1. Introduction

In the field of UAV radar signal interference, industrial UAV communication security [1], and precise and efficient UAV positioning [2,3], accurate recognition of modulation types in UAV radar signals is of paramount importance. It facilitates the assessment of signal threat levels and enables the selection of suitable algorithms for estimating signal parameters [4–7]. However, the radio environment has become increasingly intricate [8], resulting in declining SNRs in radar's routine working conditions. Consequently, there is a pressing need for modulation recognition algorithms that can exhibit enhanced performance under low SNR conditions.

In recent years, researchers have actively explored various methods for the modulation recognition of UAV radar signals. Approaches leveraging time–frequency distribution features [9], entropy values [10], resemblance coefficients [11], and wavelet packet features [12] have shown promising results. Nevertheless, most existing algorithms face challenges in accurately identifying signals when the SNR is below 5 dB [13–15]. Only a limited number of algorithms have demonstrated satisfactory performance within the SNR range of 0 dB to 5 dB [16,17], while the majority of methods completely fail to function when the SNR drops below 0 dB.

These recent advancements highlight the ongoing efforts in the field of modulation recognition for UAV radar signals. While significant progress has been made, there is still

room for improvement in terms of achieving high recognition accuracy under extremely low SNR conditions. To overcome the limitations of current methods, this paper aims to present a novel approach specifically designed to operate effectively under low SNR conditions. Successful signal recognition in such scenarios necessitates the incorporation of noise suppression techniques [18–20]. The studies referenced in [19,21] employ additional denoising techniques, which can increase hardware complexity and system response time. Higher-order spectra, such as the bispectrum, have exhibited effectiveness in noise suppression while preserving rich signal characteristics. Among the various higher-order spectra, the bispectrum represents the simplest form [22]. Therefore, this paper utilizes the bispectrum to extract signal characteristics and simultaneously suppress noise, thereby enabling the recognition of UAV radar signal modulation types through the exploitation of geometric features inherent in bispectral slices. The studies referenced in [23–27] utilize deep neural networks for modulation signal recognition. However, deep neural networks require a large amount of training data and have high hardware requirements. Therefore, this paper proposes a machine-learning-based approach, employing the GA-BP neural network as a classifier, to effectively differentiate between different signals using the feature matrix obtained through signal analysis.

The superiority of the method employed in this study for recognizing modulation schemes of UAV radar signals is demonstrated as follows:

1. This method exhibits excellent performance in identifying signal modulation schemes in low signal-to-noise ratio environments.
2. It does not require preprocessing such as time synchronization or frequency synchronization; instead, it relies solely on second-order spectrum recognition, while preserving the information of the original signal.
3. The implementation complexity of this method is low, making it more easily applicable in various scenarios.

These contributions highlight the significance of this study in the field.

The paper's structure is organized as follows to present a comprehensive understanding of the proposed method. Section 2 provides an in-depth explanation of the principles underlying the bispectrum, offering an overview of its fundamental concepts. In Section 3, the characteristics extracted from bispectral slices are elucidated in detail. Section 4 focuses on the classifier employed for the feature matrix, explaining its role and methodology. The superiority of the proposed method is validated through simulation experiments presented in Section 5, along with the inclusion of important data and performance analyses. Finally, Section 6 serves as a summary, providing a comprehensive overview of the key findings and contributions of the paper.

In summary, this paper addresses the urgent need for enhanced modulation recognition of UAV radar signals under low SNR conditions within the context of complex electronic interference environment. By harnessing the power of the bispectrum and its geometric features, the proposed method aims to surpass the limitations of existing algorithms and improve the accuracy of signal classification. The results of this study have the potential to significantly contribute to the development of more robust and efficient modulation recognition systems in the field of UAV radar signal interference.

2. Signal Model and System Overview

2.1. Signal Model

A Continuous-Wave (CW) signal is a commonly used fundamental signal type, and its model can be expressed mathematically as follows (Table 1):

$$s(t) = A \cdot \text{rect}\left(\frac{t}{T}\right) e^{j2\pi f_c t} \quad 0 < t \leq T \quad (1)$$

A CW signal is a pure sine wave signal without modulation, where the frequency f_c remains constant without any variations in frequency or amplitude. Therefore, it exhibits a

narrowband peak in the frequency spectrum, with the spectral center located at the carrier frequency f_c .

Table 1. The model of unmanned aerial vehicle radar signals.

Modulation	Formula
CW	$s(t) = A \cdot \text{rect}\left(\frac{t}{T}\right) e^{j2\pi f_c t} \quad 0 < t \leq T$
FSK	$s(t) = A \cdot \sum_{i=1}^N e^{j[2\pi f_{ci}t]} g_{T_s}(t - iT_s)$
LFM	$s(t) = A \cdot \text{rect}\left(\frac{t}{T}\right) e^{j[2\pi(f_c t + \frac{\Delta f t^2}{2T})]} \quad 0 < t \leq T$
SFM	$s(t) = A \cdot \text{rect}\left(\frac{t}{T}\right) e^{j2\pi[f_c t + m_f \sin(\Delta f t / m_f)]} \quad 0 < t \leq T$

A , T , and f_c represent the amplitude, the pulse width, and the carrier frequency, respectively. Δf represents the bandwidth. m_f represents the frequency modulation index. $g(t) = 1/\sqrt{T} \text{rect}[(t - T/2)/T]$, where $\text{rect}(t)$ represents the rectangular function. T_s represents the number of symbols. N represents the width of the symbol. T_s represents the number of subpulses in the group.

CW signals are commonly used in various applications such as wireless communication, radar systems, navigation systems, testing, and measurements. The simplicity of its model expression makes it easy to analyze and process. It is important to note that in practical applications, the specific parameters and characteristics of CW signals may be adjusted according to the requirements of the application, such as adjusting the amplitude, phase, or frequency. The above expression provides a general representation, but the specific CW signal model may vary depending on the application scenario.

A Frequency-Shift Keying (FSK) signal is a digital modulation technique where information is encoded and transmitted by changing the signal’s frequency. The FSK signal can be represented by the following mathematical expression (Table 1):

$$s(t) = A \cdot \sum_{i=1}^N e^{j[2\pi f_{ci}t]} g_{T_s}(t - iT_s) \tag{2}$$

In FSK modulation, different waveforms are modulated on different carrier frequencies to represent different binary values. FSK signals find widespread applications in wireless communication, data transmission, and modulation/demodulation systems. Their simple mathematical expression and good immunity to interference make FSK a commonly used digital modulation technique.

A Linear Frequency Modulation (LFM) signal is a modulation signal characterized by a continuous variation in frequency, commonly used in radar systems and communication systems. The mathematical expression of an LFM signal can be represented as follows (Table 1):

$$s(t) = A \cdot \text{rect}\left(\frac{t}{T}\right) e^{j[2\pi(f_c t + \frac{\Delta f t^2}{2T})]} \quad 0 < t \leq T \tag{3}$$

The key characteristic of an LFM signal is its linearly changing frequency, where the frequency increases or decreases at a constant rate over time. This linear frequency change results in a wideband signal with a continuous bandwidth in the frequency domain. LFM signals are commonly used in radar applications for range and velocity measurements, as well as for analyzing the distance and velocity of target echoes. It is important to note that the model expression of an LFM signal can be adjusted and modified based on specific application requirements, such as incorporating phase terms or pulse compression techniques. The provided expression offers a general representation, but the specific LFM signal model may vary depending on the application scenario and system design.

Sinusoidal Frequency Modulation (SFM) is a type of frequency modulation technique where the frequency of a carrier signal is varied sinusoidally with time. It is commonly used in communication systems, radar applications, and signal processing. The SFM signal model can be expressed as follows (Table 1):

$$s(t) = A \cdot \text{rect}\left(\frac{t}{T}\right) e^{j2\pi[f_c t + m_f \sin(\Delta f t / m_f)]} \quad 0 < t \leq T \quad (4)$$

SFM finds applications in various areas, including wireless communication, radar systems, audio synthesis, and frequency modulation (FM) broadcasting. By modulating the carrier frequency, SFM allows the transmission of information in the form of frequency variations, which can be demodulated at the receiver end to recover the original message or data. It is important to note that the specific implementation of SFM may vary depending on the system requirements and the desired modulation characteristics. Different modulation functions and modulation indices can be used to achieve specific frequency modulation profiles and meet the needs of the application.

2.2. System Overview

As illustrated in Figure 1, this paper proposes a comprehensive radar signal intra-pulse modulation recognition system, comprising two crucial components: signal processing and the GA-BP classifier.



Figure 1. The structure diagram of the recognition system.

Initially, the received radar signal undergoes down-conversion to an intermediate frequency. The signal processing module then employs advanced techniques to compute the bispectrum of the intermediate-frequency signals. Additionally, the module employs bilinear interpolation to resize the resulting image to an appropriate size. This resizing process ensures that the image retains the high-order characteristics of the original signals, while effectively reducing the noise to a significant extent. To achieve precise and accurate modulation recognition, the system incorporates the GA-BP classifier. This classifier has been meticulously trained offline using a deep residual network. As a result, it can proficiently classify various radar signals with exceptional accuracy. The proposed system addresses the challenges associated with radar signal modulation recognition by integrating innovative signal processing methodologies and the powerful GA-BP classifier. By leveraging bispectrum analysis, image resizing, and deep residual network training, the system achieves remarkable recognition performance, enabling the accurate identification of diverse radar signal modulations.

3. Bispectrum Estimation

The remaining noise primarily consists of the thermal noise from the receiver system and the clutter noise resulting from signal pre-processing in the reconnaissance system. Research has shown that the distribution of clutter noise, caused by a large number of scattering points, and the thermal noise from the receiver system tend to follow a Gaussian distribution [28]. Moreover, studies [29,30] demonstrate that the higher-order spectrum, as an analytical tool for time series, effectively suppresses Gaussian noise while preserving the characteristics of signals.

For instance, the power spectrum, also referred to as the second-order spectrum, is obtained through the one-dimensional Fourier transformation of the second-order cumulant of a signal. It provides valuable insights into the distribution of signal energy across different frequencies. Nevertheless, the power spectrum encounters certain limitations, including issues of equivalence and multiplicity. It primarily captures the fundamental aspects of the signal, but fails to identify the characteristics of a minimum phase system, and remains susceptible to the influence of noise. To overcome these limitations, the

utilization of higher-order spectra becomes essential. The higher-order spectra offer a more comprehensive understanding of the signal, thanks to their nonlinear system identification properties, ability to retain phase information, and effectiveness in eliminating Gaussian noise. Thus, high-order statistics serve as an indispensable mathematical tool in the field of signal processing.

As the order of the higher-order spectra increases, the computational complexity also escalates. Among the various higher-order spectra, the third-order spectrum has gained considerable attention due to its straightforward processing approach and lower computational burden. The bispectrum is mathematically defined as the two-dimensional Fourier transform of the third-order cumulant. However, its physical interpretation is not clearly defined. The normalized second-order zero-delay cumulant represents the variance of the signal, while the normalized third-order zero-lag cumulant represents the skewness of the signal. Similarly, the normalized fourth-order zero-lag cumulant represents the kurtosis of the signal. Consequently, the power spectrum can be understood as the decomposition of signal variance in the frequency domain, whereas the bispectrum represents the decomposition of signal skewness in the frequency domain. The bispectrum, based on higher-order cumulants, is defined as follows.

For a random sequence $\{x(n), x(n + T_1), \dots, x(n + T_{k-1})\}$, the higher-order cumulant $c_{kx}(T_1, \dots, T_{k-1})$ of the sequence meets [31]:

$$\sum_{T_1=-\infty}^{\infty} \dots \sum_{T_{k-1}=-\infty}^{\infty} |c_{kx}(T_1, \dots, T_{k-1})| < \infty \tag{5}$$

Then, $(k - 1)$ -dimension discrete Fourier transform (DFT) of k -order cumulant is a k -order spectrum as

$$S_{kx}(\omega_1, \dots, \omega_{k-1}) = \sum_{T_1=-\infty}^{\infty} \dots \sum_{T_{k-1}=-\infty}^{\infty} c_{kx}(T_1, \dots, T_{k-1}) \exp^{-j(\omega_1 T_1 + \dots + \omega_{k-1} T_{k-1})} \tag{6}$$

where $|\omega_i| < \pi, i = (1, \dots, k - 1), |\omega_1 + \omega_2 + \dots + \omega_{k-1}| \leq \pi$.

Bispectrum is also known as three-order bispectrum, the definition of which is as follows:

$$B_x(\omega_1, \omega_2) = \sum_{T_1=-\infty}^{\infty} \sum_{T_2=-\infty}^{\infty} c_{3x}(T_1, T_2) \exp^{-j(\omega_1 T_1 + \omega_2 T_2)} \tag{7}$$

To estimate the bispectrum of signals, this paper utilizes a direct non-parametric method for bispectrum estimation. The specific steps are as follows.

Step 1: Divide the data $\{x(0), x(1), \dots, x(N - 1)\}$ into K segments. Each segment contains M samples, $N = KM$. Overlap is allowed between data of two neighboring segments.

Step 2: Based on the classic formula, calculate the coefficients of DFT according to

$$X^{(k)}(\lambda) = \frac{1}{M} \sum_{n=0}^{M-1} x^{(k)}(n) \exp^{-j2\pi n\lambda/M} \tag{8}$$

Step 3: Then, compute the triple correlation of the coefficients calculated above according to

$$\hat{b}(\lambda_1, \lambda_2) = \frac{1}{\Delta_0^2} \sum_{i_1=-L_1}^{L_1} \sum_{i_2=-L_1}^{L_1} X^{(k)}(\lambda_1 + i_1) X^{(k)}(\lambda_2 + i_2) X^{(k)}(-\lambda_1 - \lambda_2 - i_1 - i_2) \tag{9}$$

where $k = 1, \dots, K; \lambda_1 + \lambda_2 \leq f_s/2, 0 \leq \lambda_2 \leq \lambda_1, \Delta_0 = f_s/N_0, N_0$ and L_1 should satisfy $M = 2(L_1 + 1)N_0$.

Step 4: Bispectrum estimation of data $\{x(0), x(1), \dots, x(N - 1)\}$ is given as the mean of the K segments:

$$\hat{B}(\omega_1, \omega_2) = \frac{1}{K} \sum_{k=1}^K \hat{b}(\omega_1, \omega_2) \quad (10)$$

where $\omega_1 = \frac{2\pi f_s \lambda_1}{N_0}$, $\omega_2 = \frac{2\pi f_s \lambda_2}{N_0}$.

The algorithm utilized in this study effectively computes the signal bispectrum, which exhibits superior performance in suppressing Gaussian noise and accurately capturing the unique characteristics of various radar radiation sources. To evaluate its efficacy, experimental signals from five distinct UAV radar signals, namely, CW, LFM, SFM, FSK, and noise FM, were employed. Each signal underwent extraction and analysis, employing 1024 sampling points. Figure 2 illustrates the resulting visualization, where the x and y axes represent frequency, and the z axis represents the corresponding amplitude. Notably, Figure 2 vividly showcases pronounced disparities in the bispectrum amplitude spectrum observed among radar radiation source signals employing diverse modulation modes.

Through this comprehensive investigation, it is evident that the proposed algorithm not only successfully suppresses Gaussian noise but also effectively captures the intricate nuances that differentiate radar radiation sources with distinct modulation characteristics. This finding serves to enhance our understanding and analytical capabilities in radar signal processing, fostering advancements in radar technology and applications.

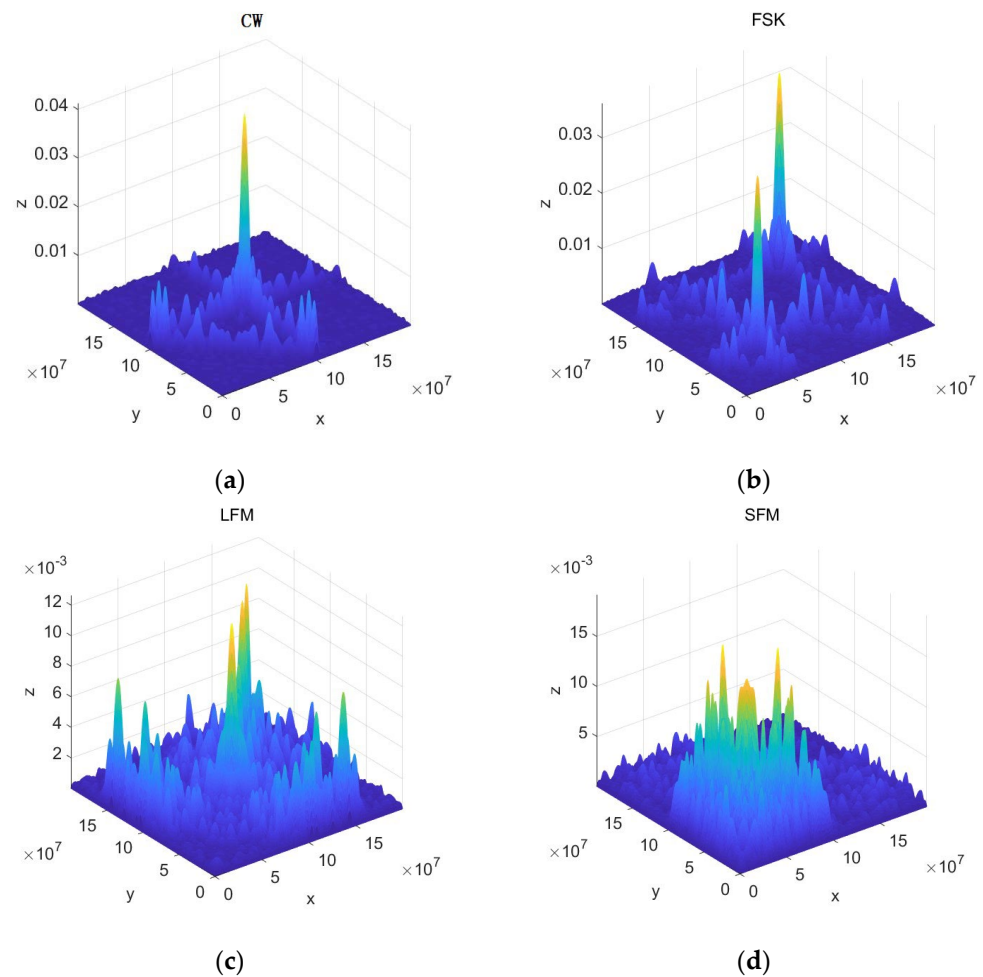


Figure 2. Cont.

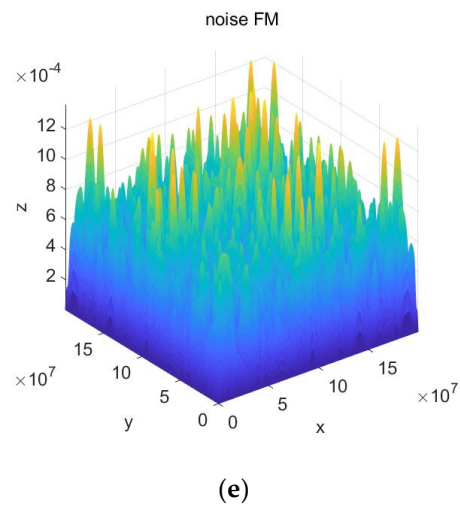


Figure 2. Bispectrum amplitude spectrum. (a) The bispectrum of CW. (b) The bispectrum of FSK. (c) The bispectrum of LFM. (d) The bispectrum of SFM. (e) The bispectrum of noise FM.

4. Characteristic Analysis of Bispectral Slices

The bispectrum amplitude spectrum serves as a valuable three-dimensional feature that captures important signal characteristics. However, its computational complexity poses a challenge for real-time processing, which limits the widespread adoption of the bispectrum in practical applications. Moreover, in signal analysis and interpretation, one-dimensional curves often offer more convenience compared to two-dimensional images. In practice, researchers commonly employ one-dimensional slices of the bispectrum to analyze specific signal characteristics or processes. The bispectral slice is obtained by performing the one-dimensional Fourier transform on the corresponding cumulant slice. Among the different types of bispectral slices, the bispectral diagonal slice is the simplest and most frequently used for analysis. The choice of bispectral slice for signal analysis is closely tied to the distribution of the signal bispectrum. Typically, in order to capture a wide range of signal features, the slice with the highest bispectral amplitude is selected. This particular slice tends to better reflect the higher-order statistical characteristics of the signal compared to other slices.

To further enhance the understanding and application of bispectrum analysis, several advanced techniques have been developed. These techniques aim to explore and extract more detailed information from the bispectrum, enabling a comprehensive analysis of signal properties. Examples include using multiple slices along different directions to reveal additional features, employing nonlinear transformations to enhance the discriminative power of the bispectrum, and utilizing adaptive approaches to handle non-stationary signals.

In summary, the bispectrum offers a powerful tool for signal analysis and characterization. Although its computational complexity and the selection of appropriate bispectral slices present challenges, ongoing research efforts continue to explore advanced techniques to overcome these limitations. By leveraging the rich information embedded in the bispectrum, researchers can gain deeper insights into the higher-order statistical properties of signals, leading to advancements in various fields such as communication systems, radar signal processing, and biomedical signal analysis.

Therefore, in this paper, the bispectral diagonal slice and bispectral horizontal slice with the maximum amplitude value are selected for analysis. Figures 3 and 4 depict both slices of the five different signals. As observed in Figures 3 and 4, the extracted bispectral slices effectively preserve the information of the bispectral amplitude spectrum. The diagonal slice and horizontal slice of the CW signal exhibit a single peak distribution, corresponding to the signal's single frequency. The diagonal slice of the FSK signal displays a bimodal distribution, reflecting its dual-frequency characteristic, while the horizontal slice shows a unimodal distribution. The diagonal slices of the LFM and SFM signals

demonstrate complex multi-peak distributions, which reflect the frequency modulation characteristics of these signals. The horizontal slices of both signals reveal differences in modulation. The diagonal and horizontal slices of the noise FM signal exhibit complex multi-peak distributions, covering the entire frequency range. Based on the distinct characteristics of the aforementioned signals, the geometric scale and distribution differences of the slices are employed in this paper to differentiate between the five types of UAV radar signals.

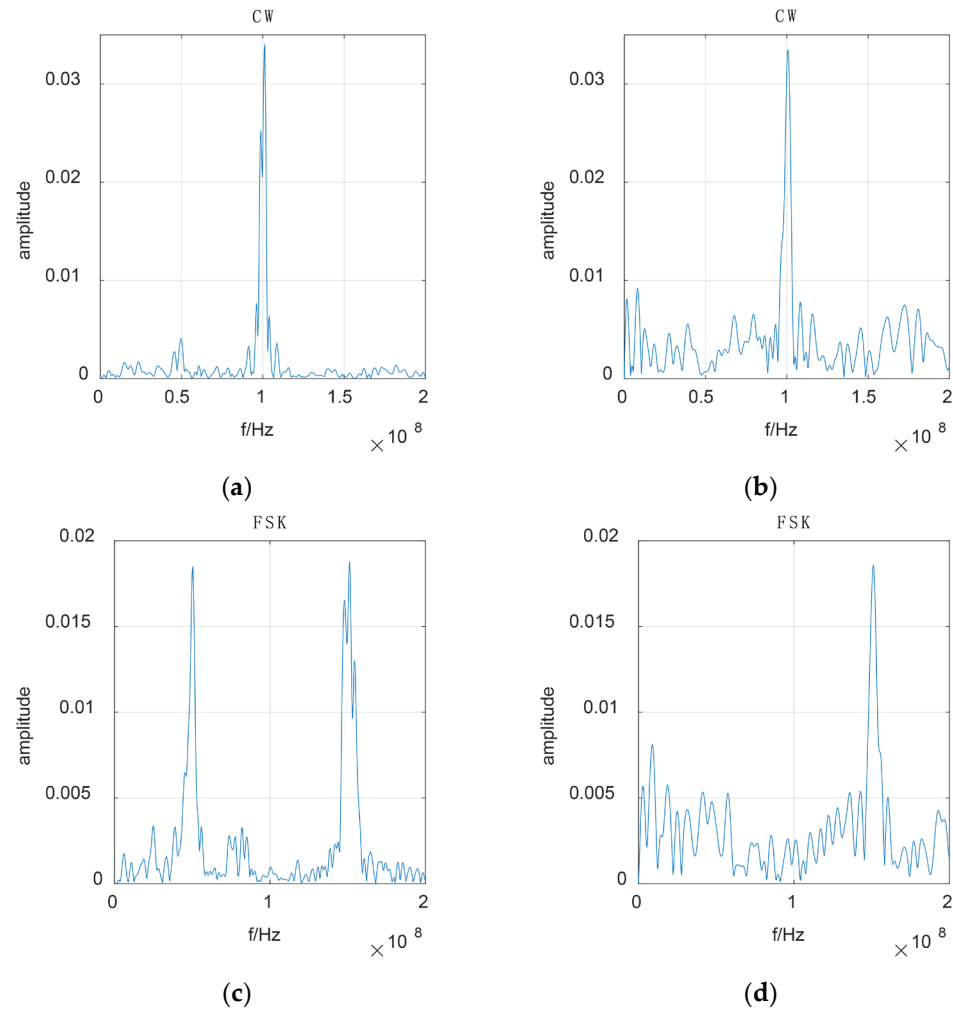


Figure 3. Bispectral slices of UAV radar signals. (a) The diagonal slice of NS. (b) The horizontal slice of NS. (c) The diagonal slice of FSK. (d) The horizontal slice of FSK.

4.1. Bispectral Convexity

The peak information of different types of UAV radar signals exhibits significant differences. To quantify the degree of deviation between the peak and the mean of these signals, the convexity T [32] of the signal's bispectral slice can be described as follows:

$$T = \frac{\max(s(\omega_1, \omega_2))}{\min(s(\omega_1, \omega_2))} \quad (11)$$

The ratio of the maximum value to the mean value in the amplitude data is referred to as the convexity T . A higher value of convexity indicates a more pronounced presence of "abnormal" features in the data. As the convexity decreases, the data tend to exhibit a more average level. Therefore, the convexity of a signal is extracted as a feature to analyze the peak distribution of the bispectrum. In this paper, the convexity of the diagonal slices and horizontal slices is extracted as features to distinguish each signal.

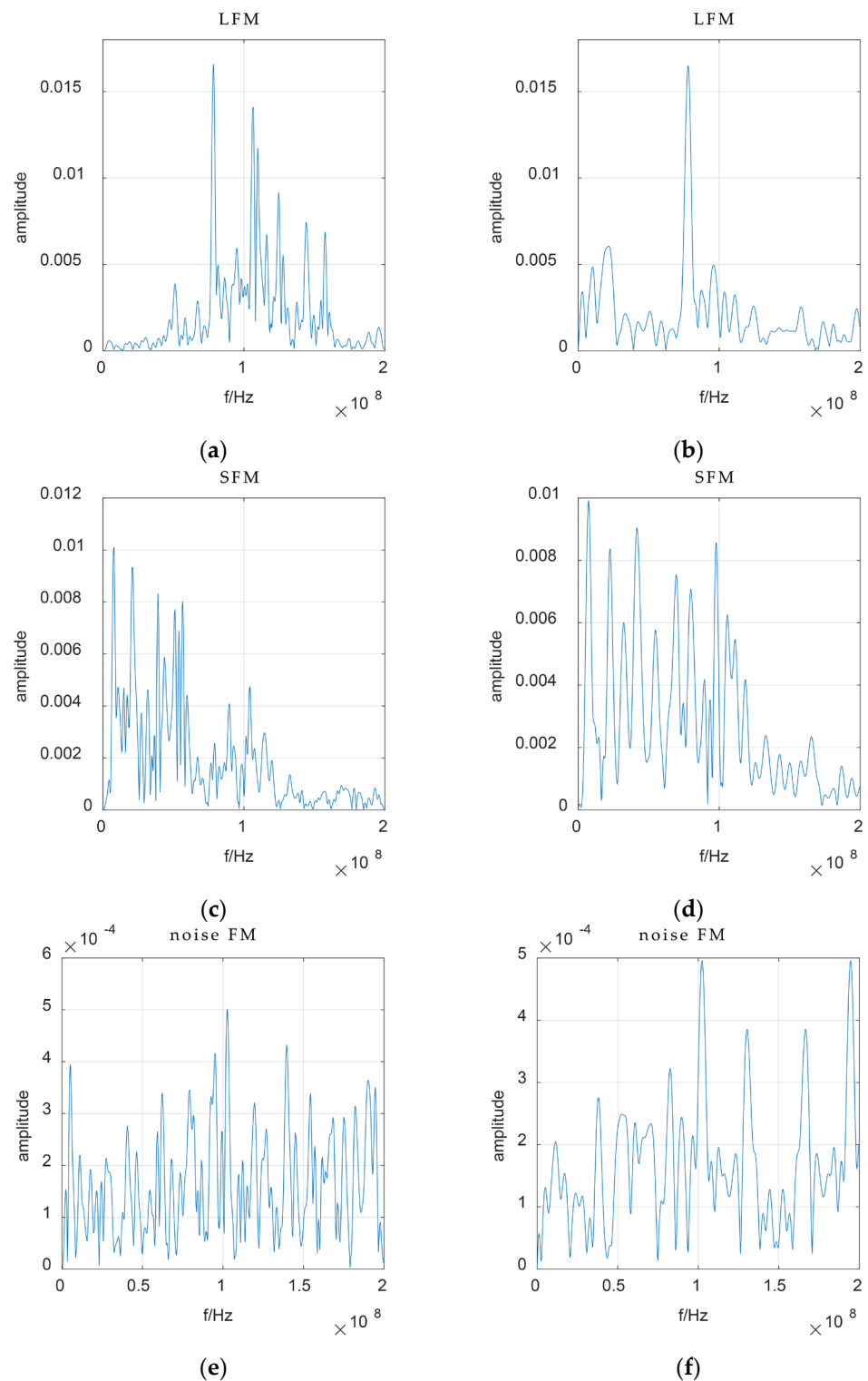


Figure 4. Bispectral slices of UAV radar signals. (a) The diagonal slice of LFM. (b) The horizontal slice of LFM. (c) The diagonal slice of SFM. (d) The horizontal slice of SFM. (e) The diagonal slice of noise FM. (f) The horizontal slice of noise FM.

4.2. Bispectral Box Dimension

The different complexity characteristics of bispectral slices reveal the distinctions among various radar radiation sources. In order to describe the differences in geometric scales, we employ the bispectral box dimension. The bispectral box dimension [33] is defined as follows:

(X, d) represents a metric space. r represents a non-negative real number. $B(c, r)$ represents a closed sphere, where c and r denote the center and radius of B , respectively. X has a non-empty subset A . For each positive number r , $M(A, r)$ denotes the number of the smallest closed spheres that cover A .

$$M(A, r) = \left\{ N : A \subset \bigcup_{i=1}^N (c_i, r) \right\} \quad (12)$$

where c_1, c_2, \dots, c_N represent different points of X .

If limit $\lim_{r \rightarrow 0} \ln(M(A, r)) / \ln M(1/r)$ exists, the box dimension of A is defined as follows [34]:

$$D_c = \lim_{r \rightarrow 0} \frac{\ln(M(A, r))}{\ln M(1/r)} \quad (13)$$

The fractal dimension of A , denoted as D_c , represents the geometric properties of bispectral slices. It is also known as the box dimension. This dimension reflects the complexity of the geometric structure. In this paper, the box dimension of the diagonal slices is extracted as a feature to describe the geometric properties.

4.3. Bispectral Sparseness

The sparseness [35,36] of a vector s is given as ξ :

$$\xi = \frac{\sqrt{L} - (\sum |s_i|) / \sqrt{\sum s_i^2}}{\sqrt{L} - 1} \quad (14)$$

where L is the length of the vector s , and $0 \leq \xi \leq 1$. The sparseness of data increases with higher values of the sparseness parameter. In this paper, the sparseness of the bispectral slices is selected as a feature to describe the characteristics of the signal.

5. Classifier Design

In this study, the GA-BP neural network is employed as the classifier to effectively distinguish between different signals, utilizing the feature matrix obtained through signal analysis.

The Genetic Algorithm (GA) is a computer-science-based method that emulates the principles of natural selection and genetic manipulation observed in biological evolution [37]. It functions as an adaptive iterative optimization algorithm with exceptional global search capabilities, aiming to improve the classification accuracy of the BP neural network and prevent it from converging to local minima [38]. By combining GA optimization with the BP neural network, the GA-BP neural network is formed.

The GA-BP neural network integrates the robustness and global optimization abilities of the GA with the learning and adaptation capabilities of the BP neural network. Initially, the GA is employed to optimize the initial weights and thresholds of the BP neural network. This optimization process enables the network to better adapt to the given signal classification task and improves its overall performance. The GA-BP algorithm flow begins with the initialization of the population, where a set of candidate solutions (chromosomes) is created. Each chromosome represents a potential set of weights and thresholds for the BP neural network. Then, the GA employs selection, crossover, and mutation operators to iteratively evolve the population and generate new and improved solutions. Through this evolutionary process, the GA explores the search space and gradually converges toward optimal solutions that maximize the classification accuracy of the BP neural network.

Overall, the integration of the GA and BP neural network in the GA-BP algorithm provides a powerful and effective approach for signal recognition tasks, leveraging the advantages of both optimization techniques and neural network learning capabilities.

The algorithm flow is illustrated in Figure 5.

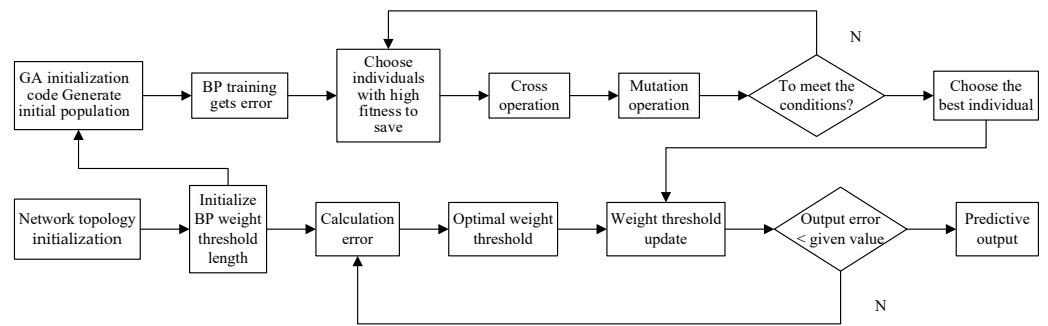


Figure 5. The flow of GA-BP algorithm.

6. Simulation Results and Analysis

Five types of typical UAV radar radiation source signals are simulated in this study: CW, FSK, LFM, SFM, and noise FM signal. The frequency and bandwidth of the simulated signals are expressed using normalized sampling frequency, with a signal length of 1024 sampling points (sampling frequency of 400 MHz). For the CW signal, the carrier frequency ranges from 0.1 to 0.4 times the sampling frequency (f_s). The FSK signal consists of two frequency points: 500 MHz and 150 MHz, with random coding as the signal's coding rule. The carrier frequencies of the LFM and SFM signals range from 0.1 to 0.4 f_s , and both signals have a bandwidth of 0.1 to 0.4 f_s . The noise FM signal has a carrier frequency of 0.1 to 0.4 f_s and a modulation index of 0.2 to 0.8 GHz/V. Additive Gaussian white noise is used as the signal noise, and the classification performance is measured with respect to the SNR. For each type of UAV radar signal, 200 samples are generated within the range of -6 to 6 dB SNR variation, with 200 samples taken every 3 dB. Among these samples, 100 are used as training samples, and the remaining samples are used as test samples. The simulation results are presented in Figure 6.

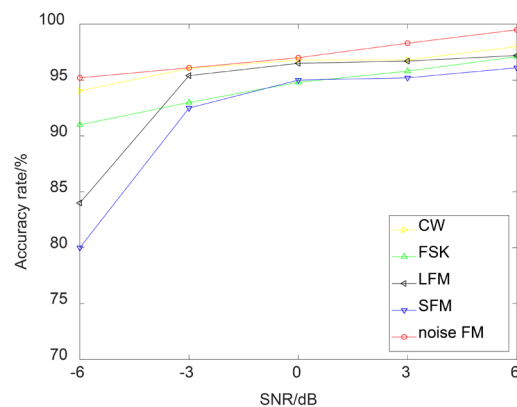


Figure 6. Sorting accuracy of UAV radar signals.

As depicted in Figure 6, the recognition rate of the five UAV radar signals exceeds 92.5% when the SNR is greater than -3 dB. Even at an SNR of -6 dB, the system maintains an accuracy rate of over 80%.

7. Conclusions

Accurate recognition of modulation types in UAV radar signals is crucial in complex electronic interference environment. This paper proposes a modulation recognition method for UAV radar signals based on bispectral slices and a GA-BP neural network. The proposed method overcomes the limitations of existing techniques, particularly in low SNR scenarios. It achieves accurate recognition of five types of UAV radar signals: CW, FSK, LFM, SFM, and FM. Notably, even in low SNR environments with an SNR set to -3 dB, the proposed method achieves a recognition accuracy of 92.5% for these five different

UAV radar signals. However, our method has certain limitations, such as its inability to effectively differentiate signals other than these five types. In our future work, we will focus not only on the recognition of the signals of interest but also on rejecting other unknown and irrelevant signals.

Author Contributions: Conceptualization, S.C.; Methodology, Y.S.; Software, K.C. and B.S.; Formal analysis, S.Y.; Writing—original draft, X.L. All authors have read and agreed to the published version of the manuscript.

Funding: 1—Special Project on Governmental International Science and Technology Innovation Cooperation under the National Key Research and Development Program: 2022YFE0122300; 2—National Natural Science Foundation of China under Grant 61801220.

Institutional Review Board Statement: Not applicable.

Informed Consent Statement: Oral consent has been obtained from all research participants.

Data Availability Statement: Not applicable.

Conflicts of Interest: The authors declare no conflict of interest.

References

1. Tan, Y.; Wang, J.; Liu, J.; Kato, N. Blockchain Assisted Distributed and Lightweight Authentication Service for Industrial Unmanned Aerial Vehicles. *IEEE Internet Things J.* **2022**, *9*, 16928–16940. [[CrossRef](#)]
2. Wen, F.; Ren, D.; Zhang, X.; Gui, G.; Adebisi, B.; Sari, H.; Adachi, F. Fast Localizing for Anonymous UAVs Oriented Toward Polarized Massive MIMO Systems. *IEEE Internet Things J.* **2023**, *1*. [[CrossRef](#)]
3. Wen, F.; Shi, J.; Gui, G.; Gacanin, H.; Dobre, O.A. 3-D Positioning Method for Anonymous UAV Based on Bistatic Polarized MIMO Radar. *IEEE Internet Things J.* **2023**, *10*, 815–827. [[CrossRef](#)]
4. Latombe, G.; Granger, E.; Dilkes, F.A. Fast Learning of Grammar Production Probabilities in Radar Electronic Support. *IEEE Trans. Aerosp. Electron. Syst.* **2010**, *46*, 1262–1289. [[CrossRef](#)]
5. Kim, S.; Kim, J.; Lee, S. Modulation type classification of interference signals in automotive radar systems. *IET Radar Sonar Navig.* **2019**, *13*, 944–952. [[CrossRef](#)]
6. Wei, S.; Qu, Q.; Su, H.; Wang, M.; Shi, J.; Hao, X. Intra-pulse modulation radar signal recognition based on CLDN network. *IET Radar Sonar Navig.* **2020**, *14*, 803–810. [[CrossRef](#)]
7. Kim, J.; Lee, S.; Kim, Y.-H.; Kim, S. Classification of Interference Signal for Automotive Radar Systems with Convolutional Neural Network. *IEEE Access* **2020**, *8*, 176717–176727. [[CrossRef](#)]
8. Chen, K.; Zhang, J.; Chen, S.; Zhang, S.; Zhao, H. Active Jamming Mitigation for Short-Range Detection System. *IEEE Trans. Veh. Technol.* **2023**, 1–12. [[CrossRef](#)]
9. Ren, M.; Cai, J.; Zhu, Y. Classification of radar signals using time-frequency transforms and fuzzy clustering. In Proceedings of the 2010 International Conference on Microwave and Millimeter Wave Technology, Chengdu, China, 8–11 May 2010; pp. 2067–2070.
10. Ge, J.; Li, C. Multi-radar hybrid detection algorithm based on information entropy. In Proceedings of the 2016 CIE International Conference on Radar (RADAR), Guangzhou, China, 10–13 October 2016; pp. 1–4.
11. Wei, X.; Pan, Y.; Han, J.; He, H. Radar signal sorting based on resemblance coefficient of Welch power spectrum. In Proceedings of the 2017 4th International Conference on Systems and Informatics (ICSAI), Hangzhou, China, 11–13 November 2017; pp. 1120–1125.
12. Tran, V.P.; Al-Jumaily, A.A. Non-contact Doppler radar based prediction of nocturnal body orientations using deep neural network for chronic heart failure patients. In Proceedings of the 2017 International Conference on Electrical and Computing Technologies and Applications (ICECTA), Ras Al Khaimah, United Arab Emirates, 21–23 November 2017; pp. 1–5.
13. Cao, Y.; Bai, J.; Li, H.; Zhao, J.; Li, S.; Gao, Z. Deep representation method for radar emitter signal using wavelet packets decomposition. *J. Eng.* **2019**, *19*, 6282–6286. [[CrossRef](#)]
14. Chen, C.; He, M.; Xu, J.; Han, J. A New Method for Sorting Unknown Radar Emitter Signal. *Chin. J. Electron.* **2014**, *23*, 499–502.
15. Xie, L.; Wan, Q. Automatic Modulation Recognition Using Compressive Cyclic Features. *Algorithms* **2017**, *10*, 92. [[CrossRef](#)]
16. Al-Nuaimi, D.H.; Hashim, I.A.; Abidin, I.S.Z.; Salman, L.B.; Isa, N.A.M. Performance of Feature-Based Techniques for Automatic Digital Modulation Recognition and Classification—A Review. *Electronics* **2019**, *8*, 1407. [[CrossRef](#)]
17. Liu, G.; Zhang, J.; Gao, X.; Li, X. A novel deep learning approach for modulation recognition of low SNR radar signals. *IET Radar Sonar Navig.* **2020**, *14*, 1433–1439.
18. Qu, Z.; Mao, X.; Deng, Z. Radar Signal Intra-pulse Modulation Recognition Based on Convolutional Neural Network. *IEEE Access* **2018**, *6*, 43874–43884. [[CrossRef](#)]
19. Chen, K.; Zhang, S.; Zhu, L.; Chen, S.; Zhao, H. Modulation Recognition of Radar Signals Based on Adaptive Singular Value Reconstruction and Deep Residual Learning. *Sensors* **2021**, *21*, 449. [[CrossRef](#)]

20. Yu, H.; Yan, X.; Liu, S.; Li, P.; Hao, X. Radar emitter Multi-label recognition based on residual network. *Def. Technol.* **2022**, *18*, 410–417.
21. Chen, K.; Chen, S.; Zhang, S.; Zhao, H. Automatic modulation recognition of radar signals based on histogram of oriented gradient via improved principal component analysis. *Signal Image Video Process.* **2023**, *17*, 3053–3061. [[CrossRef](#)]
22. Huber, P.; Kleiner, B.; Gasser, T.; Dumermuth, G. Statistical methods for investigating phase relations in stationary stochastic processes. *IEEE Trans. Audio Electroacoust.* **1971**, *19*, 78–86. [[CrossRef](#)]
23. Chen, K.; Zhang, J.; Chen, S.; Zhang, S.; Zhao, H. Automatic modulation classification of radar signals utilizing X-net. *Digit. Signal Process.* **2022**, *123*, 103396. [[CrossRef](#)]
24. Chen, K.; Wang, L.; Zhang, J.; Chen, S.; Zhang, S. Semantic Learning for Analysis of Overlapping LPI Radar Signals. *IEEE Trans. Instrum. Meas.* **2023**, *72*, 1–15. [[CrossRef](#)]
25. Chen, K.; Zhang, J.; Chen, S.; Zhang, S. Deep metric learning for robust radar signal recognition. *Digit. Signal Process.* **2023**, *137*, 104017. [[CrossRef](#)]
26. Chen, K.; Zhang, J.; Chen, S.; Zhang, S.; Zhao, H. Recognition and Estimation for Frequency-Modulated Continuous-Wave Radars in Unknown and Complex Spectrum Environments. *IEEE Trans. Aerosp. Electron. Syst.* **2023**, 1–14. [[CrossRef](#)]
27. Chen, K.; Zhang, J.; Zhang, S.; Chen, S.; Ma, Y. EMRNet: Efficient Modulation Recognition Networks for Continuous-Wave Radar Signals. *IEICE Trans. Electron.* **2023**, *E106–C*, 2022ECS6006. [[CrossRef](#)]
28. Helstrom, C. Distribution of the sum of clutter and thermal noise. *IEEE Trans. Aerosp. Electron. Syst.* **2000**, *36*, 709–713. [[CrossRef](#)]
29. Yuan, J. Tests of Gaussianity and linearity for random fields using estimated higher order spectra. *IEEE Trans. Signal Process.* **1998**, *46*, 247–250. [[CrossRef](#)]
30. Chen, K.; Zhu, L.; Chen, S.; Zhang, S.; Zhao, H. Deep residual learning in modulation recognition of radar signals using higher-order spectral distribution. *Measurement* **2021**, *185*, 109945. [[CrossRef](#)]
31. Kang, N.; He, M.; Han, J.; Wang, B. Radar emitter fingerprint recognition based on bispectrum and SURF feature. In Proceedings of the 2016 CIE International Conference on Radar (RADAR), Guangzhou, China, 10–13 October 2016; pp. 1–5.
32. Wei, D.; Zhang, S.; Chen, S.; Zhao, H.; Zhu, L. Research on Anti-Jamming Technology of Chaotic Composite Short Range Detection System Based on Underdetermined Signal Separation and Spectral Analysis. *IEEE Access* **2019**, *7*, 42298–42308. [[CrossRef](#)]
33. He, T.; Yu, K.; Chen, L.; Lai, K.; Yang, L.; Wang, X.; Zhai, Z. Image classification and recognition method to mechanical parts based on fractal dimension. In Proceedings of the 2017 International Conference on Mechanical, System and Control Engineering (ICMSEC), St. Petersburg, Russia, 19–21 May 2017; pp. 63–66.
34. Hongbin, G.; Weiyi, P.; Chunru, H.; Yongqiang, Z. A Speech Endpoint Detection Based on Dynamically Updated Threshold of Box-Counting Dimension. In Proceedings of the 2009 International Forum on Information Technology and Applications, Chengdu, China, 15–17 May 2009; pp. 397–401.
35. Rashobh, R.; Khong, A. A variable step-size multichannel equalization algorithm exploiting sparseness measure for room acoustics. In Proceedings of the 2012 IEEE International Symposium on Circuits and Systems (ISCAS), Seoul, Republic of Korea, 20–23 May 2012; pp. 2753–2756.
36. Loganathan, P.; Khong, A.; Naylor, P. A Class of Sparseness-Controlled Algorithms for Echo Cancellation. *IEEE Trans. Audio Speech Lang. Process.* **2009**, *17*, 1591–1601. [[CrossRef](#)]
37. Liu, Y.; Zhu, X.; Yang, J. Fault diagnosis of PV array based on optimised BP neural network by improved adaptive genetic algorithm. *J. Eng.* **2017**, *13*, 1427–1431. [[CrossRef](#)]
38. Yang, C.; Song, J. Research on hepatitis auxiliary diagnosis model based on fuzzy integral and GA-BP neural network. In Proceedings of the 2017 8th IEEE International Conference on Software Engineering and Service Science (ICSESS), Beijing, China, 24–26 November 2017; pp. 664–667.

Disclaimer/Publisher’s Note: The statements, opinions and data contained in all publications are solely those of the individual author(s) and contributor(s) and not of MDPI and/or the editor(s). MDPI and/or the editor(s) disclaim responsibility for any injury to people or property resulting from any ideas, methods, instructions or products referred to in the content.